



HAL
open science

Detecting the thermal aureole of a magmatic intrusion in immature to mature sediments: a case study in the East Greenland Basin (73 ° N)

Charles Aubourg, Isabelle Techer, Laurent Geoffroy, Norbert Clauer, François Baudin

► **To cite this version:**

Charles Aubourg, Isabelle Techer, Laurent Geoffroy, Norbert Clauer, François Baudin. Detecting the thermal aureole of a magmatic intrusion in immature to mature sediments: a case study in the East Greenland Basin (73 ° N). *Geophysical Journal International*, 2014, 196 (1), pp.160-174. 10.1093/gji/ggt396 . hal-00903412

HAL Id: hal-00903412

<https://hal.science/hal-00903412>

Submitted on 13 Jul 2017

HAL is a multi-disciplinary open access archive for the deposit and dissemination of scientific research documents, whether they are published or not. The documents may come from teaching and research institutions in France or abroad, or from public or private research centers.

L'archive ouverte pluridisciplinaire **HAL**, est destinée au dépôt et à la diffusion de documents scientifiques de niveau recherche, publiés ou non, émanant des établissements d'enseignement et de recherche français ou étrangers, des laboratoires publics ou privés.



Distributed under a Creative Commons Attribution - NonCommercial - NoDerivatives 4.0 International License

Detecting the thermal aureole of a magmatic intrusion in immature to mature sediments: a case study in the East Greenland Basin (73°N)

Charles Aubourg,¹ Isabelle Techer,² Laurent Geoffroy,³ Norbert Clauer⁴ and François Baudin⁵

¹Laboratoire des Fluides Complexes et leurs Réservoirs, CNRS (UMR 75150), Université de Pau, France. E-mail: charles.aubourg@univ-pau.fr

²Laboratoire GIS/CEREGE, CNRS (UMR 6635), Université de Nîmes et d'Aix-Marseille, CEREGE, 150 rue Georges Besse, F-30035 Nîmes Cedex 1, France

³Université de Brest, CNRS, UMR 6538 Domaines Océaniques, IUEM Place N. Copernic, F-29280 Plouzané, France

⁴Laboratoire d'Hydrologie et de Géochimie de Strasbourg, CNRS-UdS (UMR 7517), Université de Strasbourg, 1 rue Blessig, F-67084 Strasbourg, France

⁵Institut des Sciences de la Terre – Paris (ISTeP), CNRS (UMR 7193), UPMC – Université Paris 06, 4 place Jussieu, F-75252 Paris Cedex 05, France

SUMMARY

The Cretaceous and Triassic argillaceous rocks from the passive margin of Greenland have been investigated in order to detect the thermal aureole of magmatic intrusions, ranging from metric dyke to kilometric syenite pluton. Rock-Eval data (T_{\max} generally <468 °C), vitrinite reflectance data ($R_0 < 0.9$ percent) and illite crystallinity data ($ICI > 0.3$), all indicate a maximum of 5km burial for the argillaceous rocks whatever the distance to an intrusion. The K–Ar dating of the clays $<2\mu\text{m}$ fraction suggests that illites are mostly detrital, except near magmatic intrusions where younger ages are recorded. To get more information about the extent of the thermal aureole, rock magnetism data were determined. At distance away from the thermal aureole of the syenite intrusion, Triassic argillaceous rocks reveal a standard magnetic assemblage compatible with their burial ($R_0 \sim 0.4$ percent). It is constituted essentially by neoformed stoichiometric magnetite (Fe_3O_4). In contrast, within the thermal aureole of the magmatic intrusions, the Cretaceous argillaceous rocks contain micron-sized pyrrhotite (Fe_7S_8), firmly identified through the recognition of Besnus transition at 35K. The thermal demagnetization of natural remanence carried by this pyrrhotite shows a diagnostic 'square shouldered' pattern, indicating a narrow grain size distribution of pyrrhotite. The extension of this diagnostic pyrrhotite maps a ~ 10 -km-thick aureole around the syenitic pluton. Away from this aureole, the magnetic assemblage is diagnostic of those found in argillaceous rocks where organic matter is mature.

Key words: Magnetic mineralogy and petrology; Continental margins: divergent; Pluton emplacement; Arctic region.

1 INTRODUCTION

Sediments intruded by a magmatic body potentially develop an aureole with minerals associated with the intrusion's thermal field. These neoformed minerals could serve as proxies for a progressive burial of these host rocks (Bishop & Abbott 1995). Alternatively, identification and characterization of these minerals can help describe hidden thermal aureoles that might have some impact on the oil generation in source rocks. Focusing strictly on magnetic minerals of rocks that consist mostly of clay-type minerals (mudstones, claystones and siltstones), varied studies have connected the occurrence of iron oxides (magnetite and hematite) or iron sulphide (pyrrhotite) with the description

of thermal aureoles (Katz *et al.* 1998; Gillett 2003). The conditions at which these mineral formed depend on the fugacity of oxygen and sulphide that prevailed when the thermal aureole developed (Gillett 2003).

It is also known that iron sulphides and iron oxides form during burial (Brothers *et al.* 1996; Cairanne *et al.* 2004; Moreau *et al.* 2005; Kars *et al.* 2012). For instance, Aubourg *et al.* (2012) have defined the contours of a magnetic diagenesis consisting of three successive magnetic windows in which greigite, magnetite and pyrrhotite formed. Greigite forms in the anoxic subsurface up to several tens of metres (Roberts *et al.* 2011), being even the predominant magnetic mineral, and issues from the detrital iron oxides that were altered and

dissolved due to bacterial activity. Crystallizing at depths of about 2km (Kars *et al.* 2012), magnetite is nanometric in size with concentration of about tens of parts per million volume (ppmv). Micron-size pyrrhotite (Fe_7S_8) forms to depths of about 8km (Rochette 1987; Crouzet *et al.* 1999; Schille *et al.* 2002). It might also be added that these neoformed minerals coexist in ranges of depths that are still under debate. Greigite becomes unstable at temperatures above 200 °C, which corresponds to a burial >8km (Roberts *et al.* 2011). Magnetite is consumed during the formation of micron-sized pyrrhotite and may disappear at depths >12km. Although most of magnetic minerals are dissolved during early diagenesis, the input of residual detrital magnetic minerals, such as magnetite (Roberts *et al.* 2012) and metamorphic-derived pyrrhotite (Hornig *et al.* 2012) can disrupt this magnetic diagenetic pattern.

In the Cretaceous argillaceous sediments from the west Greenland volcanic margin, Abdelmalak *et al.* (2012) identified an assemblage with greigite, nano-sized pyrrhotite, magnetite and goethite. They also suggested two magnetic zonations that they related to maturation of hydrocarbons. In the argillaceous rocks containing mature hydrocarbons (depth >3km), they identified magnetite and nano-sized pyrrhotite. Abdelmalak *et al.* (2012) took care of their sampling collection, avoiding as much as possible thermal aureoles that result from the intrusion of metric (dykes and sills) to kilometer-size (pluton) magmatic intrusions in the west Greenland sediments. Their rock magnetic investigation did not reveal anomalies that could have resulted from such magmatic intrusions. Since the locus of greigite and magnetite agrees with the magnetic windows proposed by Aubourg *et al.* (2012) for the magnetic zoneography of diagenetic sediments, it appeared of interest to study a thermal aureole resulting from intrusion of a magmatic body into shallow sediments in order to compare the distribution of the magnetic authigenic oxides.

So, as a complementary study of both Abdelmalak *et al.* (2012) and Aubourg *et al.* (2012) works, argillaceous rocks within the thermal aureole of kilometeric and metric magmatic intrusions from the Eastern volcanic margin of Greenland were examined. A

magnetic mineralogy study was designed to check possible variations in the pattern of magnetic diagenesis. To control the thermal expansion of the halo intrusion, the maturation of the organic matter and mineral composition of the clay fraction were also evaluated. The fine fractions of clays (<2 μm) were also dated by the K–Ar method. Overall, the evidence of organic matter and clay indicate that the burial of argillaceous series was less than 5km, without demonstrating clearly a thermal perturbation or chemical intrusion in the halo. In contrast, analysis of magnetic data shows that micron-sized pyrrhotite develops in argillaceous rocks, which are presumably in the heat halo due to pluton intrusion.

2 GEOLOGICAL FRAMEWORK

2.1 Geodynamic evolution of the NE Atlantic province

The NE Atlantic area (Fig. 1) is known to have had a complex structure and evolution. Following the Caledonian orogeny and throughout the Palaeozoic and Mesozoic times, the weak lithosphere located between the Greenland and European cratons suffered episodic periods of extension and thinning followed by long-term thermal subsidence and sedimentation. The maximum of stretching/thinning occurred at the transition between Jurassic and Cretaceous (Scheck-Wenderoth *et al.* 2007). This complex evolution contributed to build a complex rift system in the NE Atlantic with, locally, extreme crust thinning. The KT boundary was characterized by a transient regional uplift (Dam *et al.* 1998). During the Palaeocene epoch (i.e. ~C27–C26 magnetochrons), large volumes of mafic magma intruded the NE Atlantic and continental crusts, and extruded as flood basalts. In both the Baffin Bay and NE Atlantic, the breakup and earliest oceanic accretion occurred during the Eocene time (Chron 24B, age

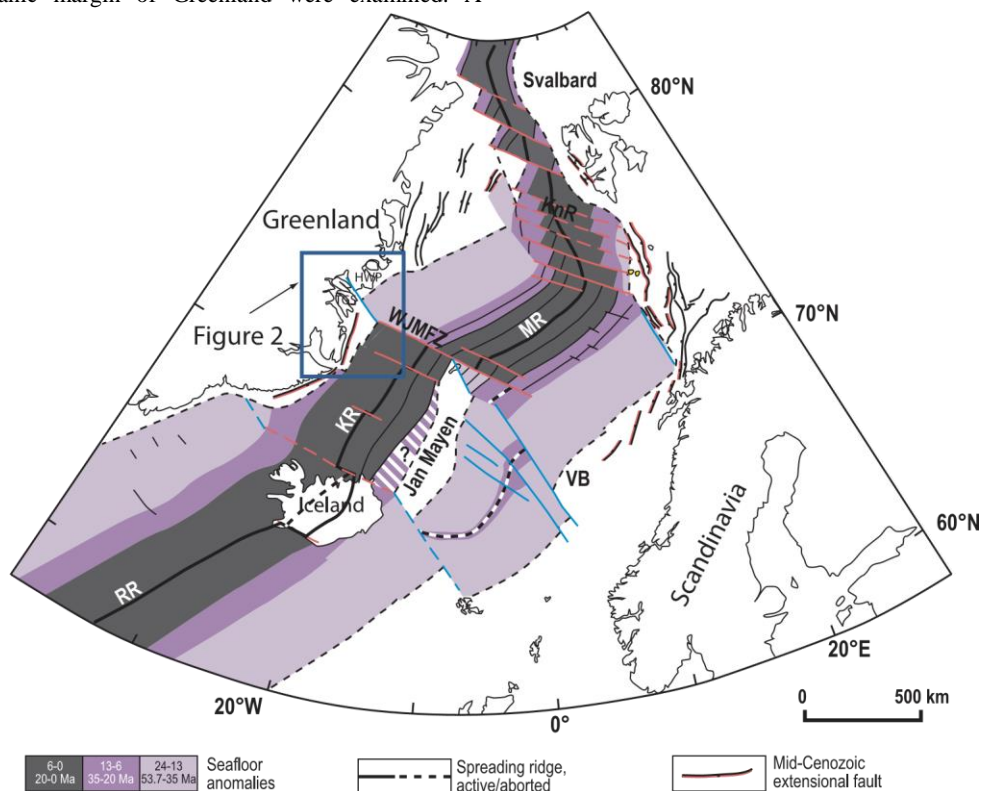


Figure 1. Simplified tectonic map of the Greenland and Norwegian seas. The box localizes the Fig. 2. Three main stages of magnetic anomalies are indicated. RR, Reykjanes Ridge; KR, Kolbeinsey Ridge; MR, Mohn Ridge; WJMFZ, West Jan Mayen Fracture Zone; VB, Voring Basin.

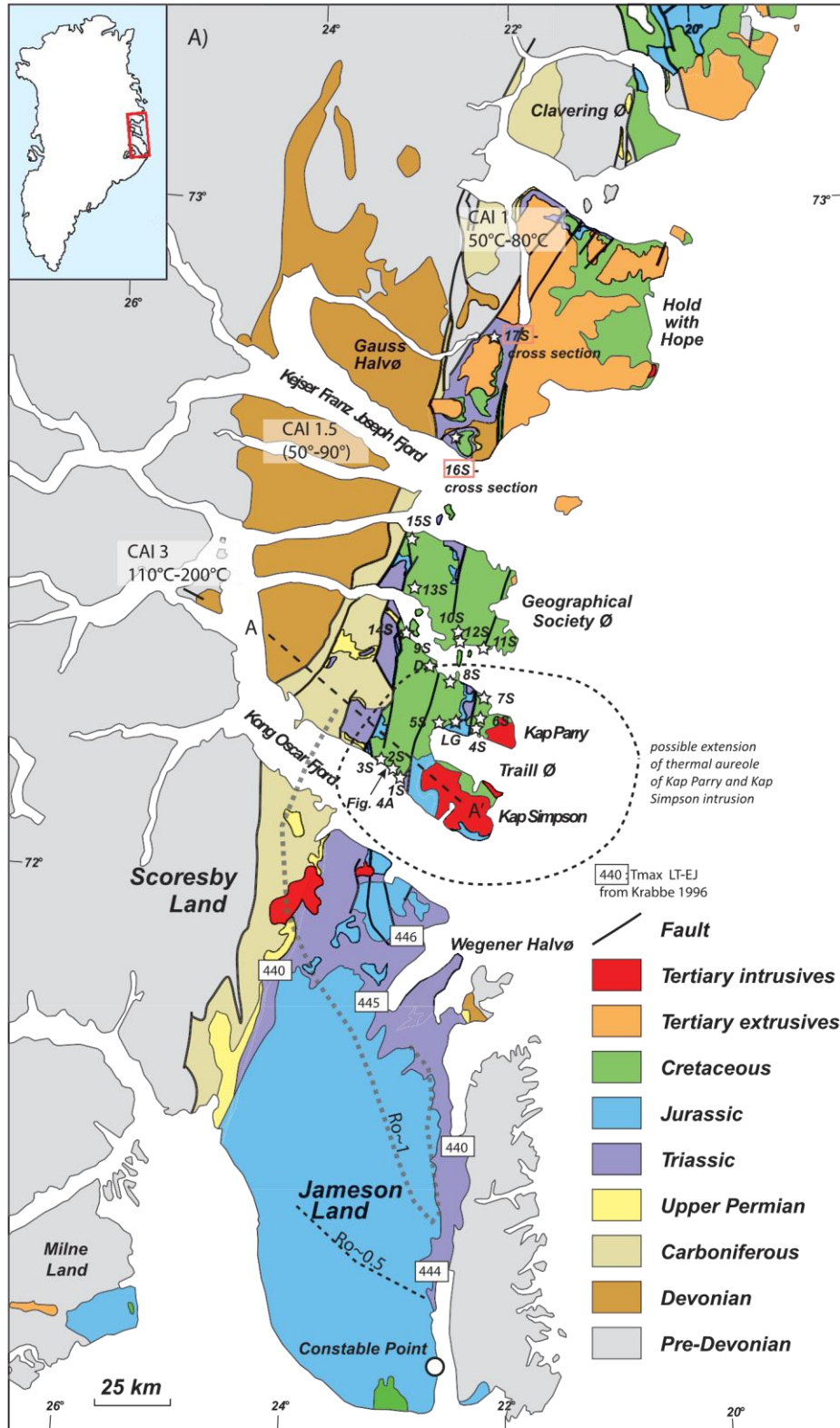


Figure 2. Simplified geological map (redrawn from Stemmerik *et al.* 1997). The stars indicate the localization of the studied sites. Maturity data from Jameson Land and from Devonian (<http://www.geus.dk/publications/review-greenland-01/gsb191p117-125.pdf>) are reported. The T_{max} values are from Krabbe (1996). The iso-values of vitrinite are from Hansen *et al.* (2001). The localization of cross section from Fig. 3 is indicated (A-A).

of the earliest oceanic magnetic anomaly at 55–57 Myr). Anomalous mantle melting continued during the breakup process although mainly focused along the breakup axes, leading to the development of volcanic passive margins.

The studied area includes the islands of Traill Ø and Geographical Society Ø, being collectively called TGS, and the Hold-with-Hope peninsula called hereafter HWH (Figs 1 and 2). The TGS and HWH

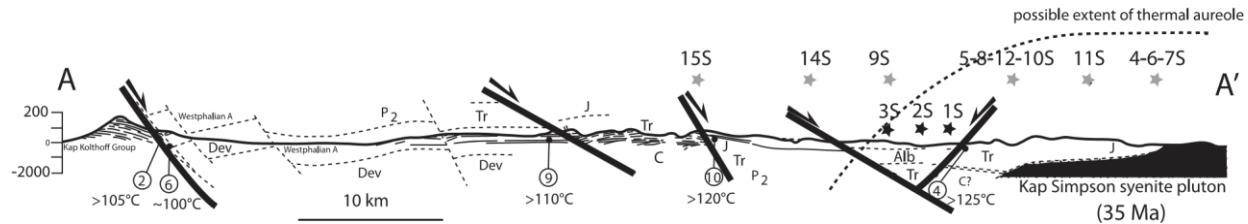


Figure 3. Cross section A–A from Fig. 2 (redraw from Thomson *et al.* (1999)). Sites (in circle) and maximum burial temperatures are from Thomson *et al.* (1999) study. The location of the sites from this study is shown (black stars, approximate location, grey stars: projected location).

represent the inner part of the NE Greenland volcanic margin (Schlindwein & Jokat 1999; Gernigon *et al.* 2004). From Late Palaeozoic to the end of the Mesozoic, TGS and HWH constituted the western edge of the NE Atlantic network of sedimentary rifts and basins. From west to east, the onshore-exposed rocks of TGS and HWH consist in a thick pile of Devonian/Lower Carboniferous (Hartz *et al.* 1997) to Upper Cretaceous sediments. The different sedimentary formations are bound by a system of eastward dipping, NNE–SSW-trending normal faults of different ages (Price *et al.* 1997; Fig. 3). Devonian to Jurassic sediments are mainly proximal continental sandstones, whose deposition seems to have been partly controlled (both during rifting and post-rifting periods) by a major boundary fault (Fig. 3; Surlyk *et al.* 1980). The Cretaceous (essentially Albian to Cenomanian) is predominantly made of dark laminated argillaceous rocks since Aptian time, with a cumulated thickness apparently not exceeding 1700 m (Surlyk *et al.* 1980).

During the Palaeocene–Eocene period, the NE Greenland basin was covered by traps and extensively intruded by mafic sills and dykes (Price *et al.* 1997). Most of the sills penetrated Cretaceous argillaceous rocks, like in the Voring Basin (Gernigon *et al.* 2004). A vertical section of ~800 m observed in the southern part of Traill Ø shows Triassic, Middle Jurassic and Cretaceous sedimentary rocks extensively intruded by dykes and sills (Fig. 4a).

The post breakup magmatic and tectonic activities of the NE Greenland basin (Upton *et al.* 1980; Price *et al.* 1997; Ellam *et al.* 1998) are perhaps correlated with the onset of the Kolbeinsey Ridge, the split of the Jan Mayen block and the functioning of the western Jan Mayen fracture zone (Fig. 1; Bott 1987; Scott 2000). Otherwise, it is a thermal residual of the former development of asthenospheric diapirs or small-scale convection cells inherited from the main Palaeocene–Eocene mantle melting event (Geoffroy *et al.* 2007). This event is associated with the emplacement of the alkaline magma at the Kap Simpson, Kap Parry and Myggbugta central complexes about ~36 Myr (Fig. 2; Upton *et al.* 1980; Price *et al.*

1997).

2.2 Burial constrains

Thomson *et al.* (1999) proposed several stages of cooling for Traill Ø, based on apatite fission tracks and vitrinite data (Fig. 2a). In

western Traill Ø, they identified a pre-Cretaceous cooling stage between 225 and 165 Myr closely related with unconformities observed within the Jurassic section. Burial temperature before this cooling event did not exceed ~140 °C. The authors also reported a second cooling event between 40 and 30 Myr that was contemporaneous with the Oligocene alkaline magmatic activity. To explain the cooling, Thomson *et al.* (1999) favoured a transient

thermal uplift in response to the passage of the Iceland plume between 40 and 30 Myr. However, they do not exclude basin-scale hydrothermal circulations in relation with setting of the Oligocene intrusions. A broad range of burial temperatures was also considered before this second cooling event, ranging from 170 °C near syenite intrusives to ~100 °C or so away from them. A third stage of cooling was set during the late Tertiary (10 to 5 Myr), which may correspond to the major episode of Tertiary exhumation, with burial temperatures before cooling below 100 °C. From this data set, one can consider that most of the Carboniferous to Jurassic rocks experienced modest temperature, within the oil window (<150 °C; Fig. 3). South of Traill Ø in the Jameson Land, the T_{max} data derived from RockEval pyrolyse of the Kap Stewart Formation (Upper Triassic–Lower Jurassic) are homogenous (440–446 °C) pointing to an early maturation stage (Fig. 2; Krabbe 1996; Mathiesen *et al.* 2000; Hansen *et al.* 2001). However, vitrinite reflectance data indicate a slight positive gradient of temperature towards the north of Jameson Island (Fig. 2). Hansen *et al.* (2001) emphasized particularly this trend on the basis of fission-track data. They envisaged that the temperature did not exceed 70 °C in the Permian–Triassic rocks of southern Jameson Land, while it was above or close to 125 °C in the northeastern Jameson Land. The age of apatite partial annealing zone is getting younger, from ~45 to ~16 Myr along a S–N transect from eastern Jameson Land to Traill Ø (Fig. 2). Fission tracks from Traill Ø and Jameson Land both suggest a slight elevation of temperature towards the syenitic pluton.

3 SAMPLING

In the studied area, the shallow marine Middle-Jurassic sandstones or Triassic clastics are uncomfortably overlain by hundreds of metres of Cretaceous argillaceous rocks (Fig. 3; Surlyk *et al.* 1980; Stemmerik *et al.* 1997). The Lower Cretaceous sequence (Aptian–Albian) consists of deepwater dark laminated argillaceous rocks with a maximum thickness of 950 m. The upper Cretaceous sequence reached more than 700 m in thickness with facies of the same type as in the lower Cretaceous. Sixteen samples of Cretaceous argillaceous rocks were collected for the TGS study, 11 sites on Traill Ø and 5 sites on Geographical Society Ø. Two additional sites of Triassic age were studied at HWH, close to the Cretaceous boundary (Fig. 2,

Table 1). Many sills and dykes intruded this stratigraphic sequence (Fig. 4). In the field, no significant disturbance of the argillaceous rocks could be observed, except in the first millimetre of the quench contact. In order to evaluate the potential imprint of the volcanic intrusions, several samples were taken up to 3 m away from a 1-m-thick dyke (9SD site, Traill Ø). In addition, at the 6S locality (Traill Ø), samples were collected few metres within the hanging wall of a thick sill dipping to the

west (Fig. 4b). At the 8S locality (Traill Ø), the sampled Cretaceous argillaceous rocks were taken at about 10 m away from metric sills. Sites 4S and 6S (Traill Ø) are located at ~5km from Kap Parry 36-Myr-old syenite (Fig. 2). Triassic sandstones at sites 16S and 17S are overlain by ~100 m of Cretaceous argillaceous rocks and Palaeocene flood basalts.

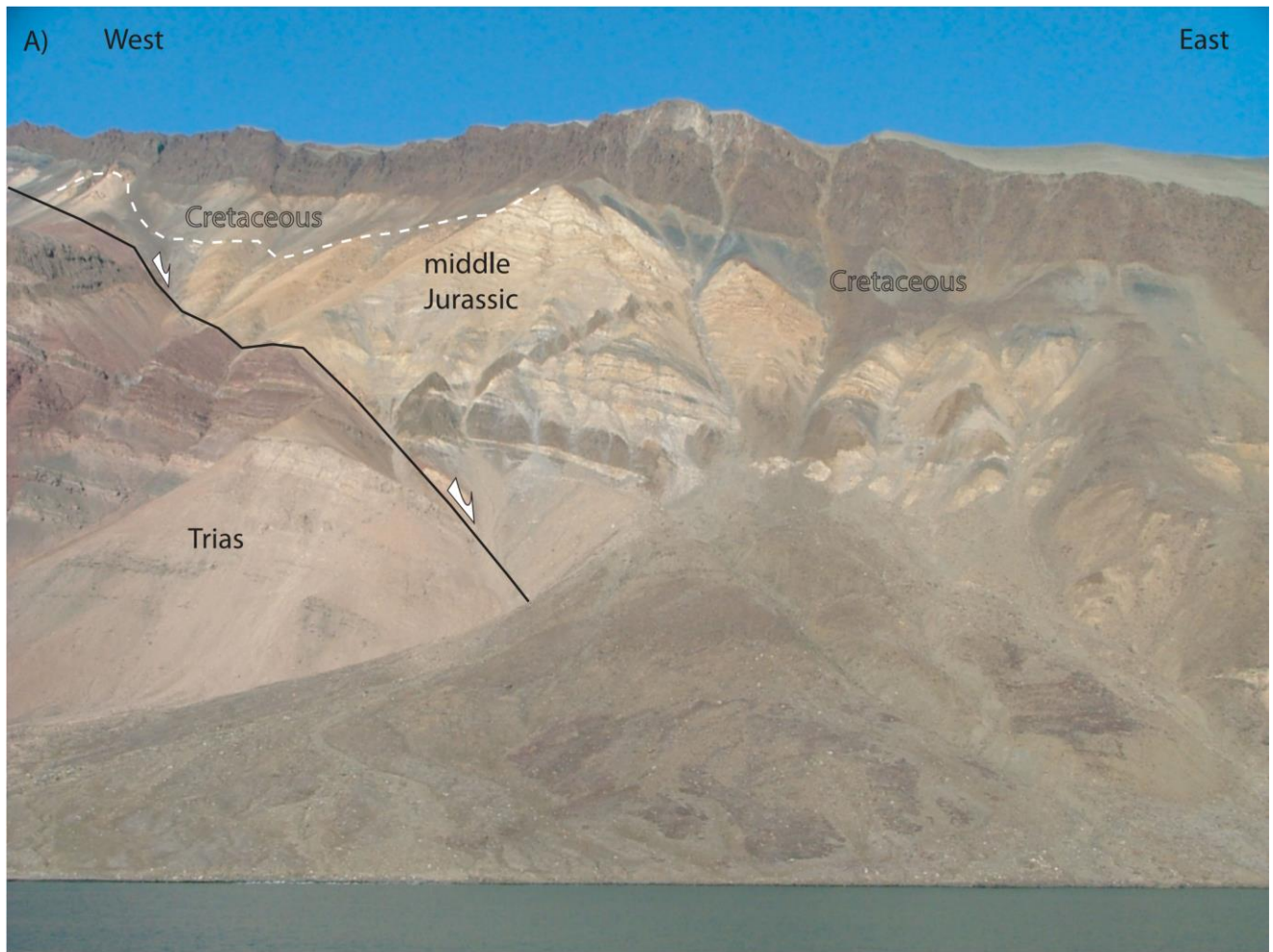


Figure 4. (a) ~800 m stratigraphic section from Permo-Triassic to Cretaceous. See location of photo on Fig. 2. Most of the Palaeocene–Eocene sills were injected within the Cretaceous argillaceous rocks. This stratigraphic pile is dissected by normal faults of various ages, some being contemporaneous of the Cretaceous deposition. (b) Near site 6S, where a large sill intruded the Cretaceous argillaceous rocks.

Table 1. Location (latitude, longitude) of the studied sites, Rock-Eval and vitrinite data (T_{max} , °C; TOC, total organic contents; R_0 , percent with standard deviation at 95 percent). Palaeomagnetism. Natural remanent magnetization (NRM) with its standard deviation at 95 percent. Drop of magnetization at 350 °C, near the Curie temperature of pyrrhotite.

Site	Latitude	Longitude	Rock-Eval		Vitrinite		Palaeomagnetism		
			T_{max} (°C)	TOC (per cent)	R_0 (per cent)	SD	NRM (A m ⁻¹)	SD	Per cent 350 °C
1S	N72°18'35.4"	W23°03'06.2"					1.9E-02	2.7E-02	78
2S	N72°20'44.5"	W23°11'10.5"	418	0.69					
3S	N72°24'24.1"	W23°29'25.5"					1.8E-01	3.0E-01	82
4S	N72°27'52.4"	W22°18'33.7"					4.6E-02	2.7E-02	96
5S	N72°29'01.5"	W22°37'30.5"					2.0E-02	1.9E-02	79
LG	N72°29'18.5"	W22°20'827"							
6S	N72°28'46.6"	W22°17'17.4"					1.2E-01	1.6E-01	70
7S	N72°33'17.8"	W22°18'02.0"					1.0E-02	1.1E-02	95
8S	N72°35'09.6"	W22°34'55.0"	600	0.37			8.8E-03	2.6E-03	82
9S	N72°37'16.5"	W22°46'36.0"	468	0.79	0.3	0			
9SD1-5	N72°37'16.5"	W22°46'36.0"	502	0.71					
9SD2-20	N72°37'16.5"	W22°46'36.0"	500	0.1					
9SD3-100	N72°37'16.5"	W22°46'36.0"	500	0.09					
9SD4-10	N72°37'16.5"	W22°46'36.0"	500	0.16					
9SD5-300	N72°37'16.5"	W22°46'36.0"	495	0.1					
10S	N72°44'08.5"	W22°23'19.5"							
11S	N72°42'17.6"	W22°07'38.2"	365	0.11			5.2E-03	3.4E-03	66
12S	N72°42'32.0"	W22°23'45.9"							
13S	N72°52'29.3"	W23°06'00.2"					1.4E-03	2.0E-03	45
14S	N72°45'39.3"	W23°04'29.7"					1.4E-03	4.2E-05	51
15S	N73°01'01.2"	W23°00'30.8"	468	0.78			2.1E-03	1.5E-03	66
	N73°01'24.1"	W22°59'13.3"	465	0.46	0.9	0.2			
16S	N73°18'49.2"	W22°32'21.7"	435	1.57	0.4	0.1	9.1E-03	8.1E-03	24
			432	0.99					
			439	2.89	0.5	0.2			
17S	N73°36'46.8"	W22°10'04.1"	439	9.66	0.4	0.1	9.7E-02	2.7E-02	80

4 METHODS

4.1 Magnetic mineralogy

The temperature dependency of remanence is probably the best mean to identify trace amounts of magnetic minerals. The main typical features of the two main minerals, namely magnetite and pyrrhotite, are displayed here. At high temperature (from room temperature to 600 °C), the maximum unblocking temperature at which magnetite and pyrrhotite lose their remanent magnetization is ~580 and ~320 °C, respectively (Dunlop 1995). At low temperature, from room temperature to tens of Kelvin (27 to -263 °C), two diagnostic transitions at 35K (Besnus transition) and 120K (Verwey transition) allow identification of pyrrhotite (Dekkers *et al.* 1989; Rochette *et al.* 1990) and stoichiometric magnetite (Ozdemir *et al.* 2002), respectively. Here, the combination of high- and lowtemperature dependency of remanent magnetization is used to control the occurrence of both, pyrrhotite and magnetite.

The natural remanent magnetization (NRM) and isothermal remanent magnetization acquired at room temperature (IRM) are thermally demagnetized using a home-made furnace shielded against Earth magnetic field. NRM and IRM are measured using a JR6 spinner magnetometer (Agico-Ltd). The IRM is imparted according to Lowrie's method (1990) along three directions of a standard 10-cc core (Z at 2.1 Tesla (T), Y at 0.5 T and X at 0.1 T). Non-oriented cores of 10.8 cc of Cretaceous and Triassic argillaceous rocks are measured

(53 cores for NRM, 2 cores for IRM).

The evolution of saturated isothermal remanent magnetization acquired at room temperature or low temperature from 300 to 5K is monitored. SIRM is acquired at room temperature (RT-SIRM) or at low temperature (LT-SIRM) with the application of a magnetic field of 2.5 T. Low-temperature procedures are standard and are described for instance in Weaver *et al.* (2002). We used: (1) the RT-SIRM procedure, characterized by the cooling from 300 to 5K of an RT-SIRM. In some samples, the warming curve was also monitored from 300 to 10K after RT-SIRM cooling and (2) the LT-SIRM procedure, characterized by the warming from 5K (or 10K) to 300K of a LT-SIRM. A supra-conducting SQUID magnetometer MPMS was used and ~400 mg of rock powder sealed in a gel cap were measured.

4.2 Rock-Eval and vitrinite reflectance

Total organic carbon content (TOC, in wt per cent), T_{max} (°C) and hydrogen index (HI, in mg hydrocarbons per g TOC) were determined by Rock-Eval_R pyrolysis (Espitalie 1993) with an Oil Show' Analyser device (Vinci Technologies, Nanterre, France). T_{max} is the temperature at maximum pyrolytic hydrocarbon generation. It varies as a function of the natural thermal maturity of the organic matter (Espitalie 1986).

Organic petrography analysis under reflected light and fluorescence was performed on polished sections of organic matter concentrated after densimetric floating. Identification of land-derived organic particles, that is, mainly from vitrinite and inertinite maceral groups, was made following the nomenclature

of Stach *et al.* (1982). Random vitrinite measurements (R_0 expressed in per cent) were made on the same densimetric concentrates under reflected light using a $\times 50$ oil immersion objective. Thirty-two macerals samples were selected for Rock-Eval pyrolysis and 17 for maceral analysis and reflectance vitrinite measurements. The precision for these analyses is ± 0.1 percent for TOC, ± 2 °C for T_{max} and ± 0.08 percent for R_0 .

4.3 X-ray and K–Ar analysis

All samples were analysed by X-ray diffraction (XRD) as whole rocks and size fractions to determine their mineral composition. The analyses were carried out on a Bruker D5000 diffractometer operated at 40 kV and 20 mA at a scanning rate of $0.02^\circ 2\theta \text{ min}^{-1}$ with $\text{CuK}\alpha$ radiation. The random powder patterns of the whole rocks were recorded from 2° to $65^\circ 2\theta$. The samples were disaggregated by crushing rock chips of about 1 cm^3 for about 2 min and by sieving the powders at 800 meshes. The carbonate components were removed by leaching the sample powders with cold 10 percent HCl. The $<2\mu\text{m}$ fraction of all samples was separated by gravity settling in distilled water, and concentration of the separated fractions by centrifugation. All size fractions were analysed as oriented mounts prepared by smearing the slurries on glass slides. Four XRD diagrams were obtained for each size fraction: after air-drying (AD), ethylene-glycol (EG) and hydrazine (Hy) treatment, and heating (He) at 490 °C during 4 hr. The samples were scanned from 2° to $30^\circ 2\theta$ for the AD and EG treated fractions and from 2° to $15^\circ 2\theta$ for the Hy and He treated fractions. The identification of the types of the illite-smectite mixed layers (I-S) was based on XRD-pattern decomposition using the DECOMPXR program (Lanson 1997) and on the procedures described by Moore & Reynolds (1997). The percentage of illite in I-S was determined by the position of the second and/or third reflections (near $10.3\text{--}8.9^\circ 2\theta$ and $16.4\text{--}17.8^\circ 2\theta$, respectively) on the decomposed XRD patterns of the EG treated fractions. The relative abundance of the different clay types was estimated from peak area after peak decomposition of the different size fractions (Lanson & Besson 1992). The Illite Crystallinity Index (ICI), also called 'full width at half maximum' (FWHM) was also determined. Based on the measurement of the width of the d_{001} XRD peak at half high it gives a good idea about the degree of crystallization of the illite-type particles: the peak's width decreases, when burial temperature increases (Kubler 1966; Frey 1987). In fact, the decrease in width at half maximum that is to say in the crystallinity, relates to a decrease in expandability of the interlayer space of the smectite-type layers that incorporate progressively K to tend towards a non-expandable illite end-member.

The K–Ar determinations considered as exploratory were made on the $<2 \mu\text{m}$ fractions using a procedure close to that reported by Bonhomme *et al.* (1975). Potassium was measured by flame spectrophotometry with an accuracy of ± 1.5 per cent. For the Ar analyses, the samples were preheated under vacuum at 100 °C for at least 12 hr to reduce the amount of atmospheric Ar adsorbed on the mineral surfaces during sample preparation and handling. The results were controlled by repetitive analysis of the GL-O international standard, which averaged 24.99 ± 0.10

$\times 10^{-6} \text{ cm}^3 \text{ g}^{-1} \text{ STP}$ (2σ) of radiogenic ^{40}Ar for 4 determinations during the course of the study. The $^{40}\text{Ar}/^{36}\text{Ar}$ ratio of atmospheric Ar was also measured periodically and averaged 291.1 ± 2.2 (2σ) for six determinations during the course of the study. The usual decay constants were used for the age calculations (Steiger & Jager 1977), and the global error was evaluated to be systematically better than 2 percent (2σ).

5 RESULTS

5.1 Magnetic mineralogy

5.1.1 Thermal demagnetization of NRM and IRM

The magnitude of NRM displays variations of three orders of magnitude (from 10^{-1} to 10^{-4} A m^{-1} , Table 1). Relationships between magnitude of magnetization and distance to magmatic intrusion were not clearly detected. The thermal demagnetization of NRM outlines three distinct behaviours of the samples that are labelled P, M and PM. As will be discussed further, P and M refer, respectively to pyrrhotite and magnetite. The drop of NRM at 350°C for all samples is indicated in Table 1. For P-behaviour (observed for instance in the 5S sample), the demagnetization process leads to the setting of a plateau between room temperature and $\sim 300^\circ\text{C}$, which is followed by a significant drop (40–100 percent) at $\sim 350^\circ\text{C}$ (Fig. 5a, Table 1). For the PM-behaviour (17S sample for instance), a significant loss of magnetization is observed between room temperature and 350°C (40–85 percent NRM), without development of a plateau as for the P-pattern (Fig. 5a). The maximum unblocking temperature ranges between 500 and 600°C when interpolating the trend of the demagnetization curve. For the M-behaviour (15S sample), the pattern of NRM demagnetization curve is single with a convex shape directed to the top and a maximum unblocking temperature in the range 600 – 700°C . About 80 percent of NRM is demagnetized at 600°C , suggesting that the mineral assemblage is a mixture of magnetite and hematite (Fig. 5a). At 350°C , a loss from a few percents up to 65 percent of NRM is observed.

The P-behaviour with a maximum unblocking temperature between 300 and 350°C is generally attributed to the contribution of an Fe-sulphide, such as greigite (Fe_3S_4 , Curie temperature $\sim 350^\circ\text{C}$) or monoclinic pyrrhotite (Fe_7S_8 , Curie temperature $\sim 320^\circ\text{C}$). The PM-

behaviour likely results from a combined contribution of Fe-sulphides and magnetite.

These behaviours allow distinction of three groups labelled A, B and C among the studied samples. For group A, that includes the sites 1S, 4S, 5S, 7S, 8S and 11S, most samples display a P-behaviour. For group C represented essentially by the site 15S, sample displays the M behaviour. For group B that includes the sites 3S, 6S, 13S, 14S, 16S and 17S, the PM and M-behaviours are combined.

The thermal demagnetization of NRM showed unequivocally that magnetite is present as a magnetic carrier in almost all sites, and more specifically at the sites where the groups B and C were described. High-temperature IRM experiments were combined on the samples of sites 5S (group A) and 17S (group B; Figs 5b and c). The demagnetization pattern of composite IRM resembles that of NRM. One main mineral was detected for the sample of site 5S characterized by a soft coercivity ($H_c < 0.1 \text{ T}$) and a maximum unblocking temperature of $\sim 320^\circ\text{C}$ (Fig. 5b). These characteristics are diagnostic of Fe-sulphide. However, it might be added that the ~ 10 percent of residual IRM shows an unblocking temperature close to 600°C (when the interpolating trend ranges from 350 to 500°C). It means that a small amount of magnetite coexists with Fe-sulphide at the site 5S. For the sample of site 17S, the pattern is different apparently with an assemblage of magnetic minerals with harder coercivities in average (Fig. 5c). The overall maximum unblocking temperature is about 500°C , indicating that magnetite is present. But the occurrence of break-in-slopes at $\sim 300^\circ\text{C}$ for the intermediate coercivity suggests the presence of a Fe-sulphide. These two examples of high-temperature demagnetization of composite IRM indicate that an assemblage of magnetite and Fe-sulphide exists in the Cretaceous and Triassic argillaceous rocks, in good accordance with the pattern of the thermal NRM demagnetization.

5.1.2 Low-temperature magnetic properties

The low-temperature experiments for samples 5S and 3S from group A and sample 17S from group B are shown (Fig. 6). On cooling, the RT-SIRM reveals diagnostic magnetic transitions. A sharp Neel transition at $\sim 39\text{K}$ is observed in sample 5S with an increase of remanence (RT-SIRM and an induced magnetization) by a factor of 50:1 (Fig. 5a). This indicates the presence of siderite (FeCO_3 ; e.g. Housen *et al.* 1996). A Besnus transition is detected at $\sim 35\text{K}$ in sample 3S (Fig. 6b), which indicates the

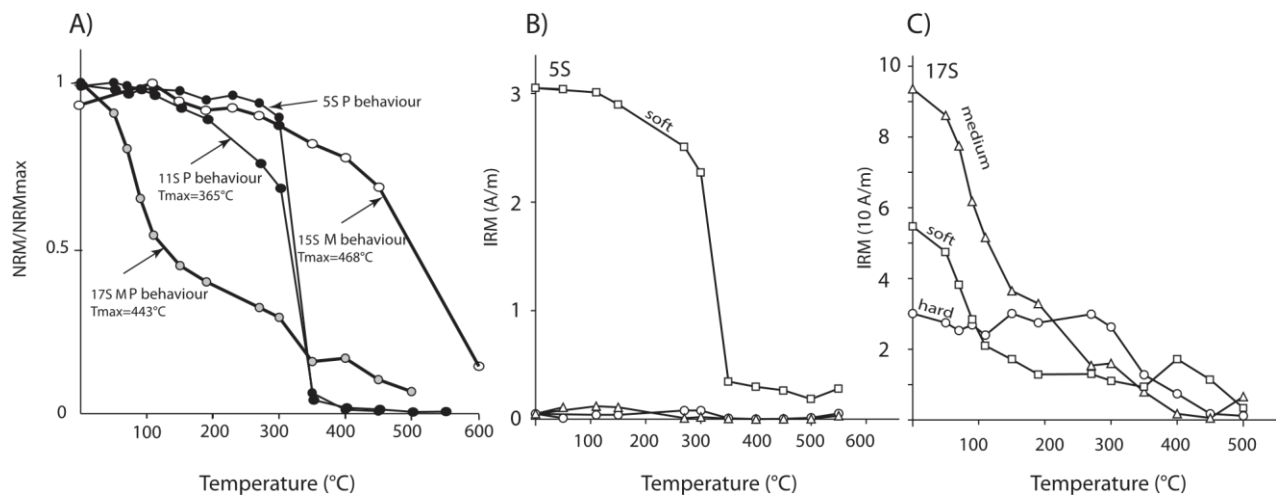


Figure 5. Thermal demagnetization of natural remanent magnetization (NRM) and isothermal remanent magnetization (IRM). (a) Thermal demagnetization of NRM. P, M and PM behaviours refer to a pattern of demagnetization discussed in the text. (b) and (c) Stepwise demagnetization of composite IRM. \square 0.1 T, medium: 0.5 T, hard: 1.2 T (b) sample from site 5S which displays the P behaviour. (c) Sample from site 17S, which displays the PM behaviour. \triangle the similitude of the NRM and IRM patterns.

occurrence of micron-sized pyrrhotite. A Verwey transition is detected at ~ 120 K in sample 17S (Fig. 6c). The Verwey transition demonstrates the occurrence of stoichiometric magnetite. On cooling, one can observe also the superimposition of a small induced magnetization and the RT-SIRM near 35 K (Fig. 6c). This transition suggests that hyper-fine fraction of both magnetite and pyrrhotite are present (Aubourg & Pozzi 2010; Kars *et al.* 2011). The pyrrhotite, if effectively present, would be nano-sized and thus not able to carry a remanence at room temperature (neither NRM nor RT-SIRM). Therefore, the iron sulphide detected in sample 17S in the course of NRM or RT-

SIRM demagnetization (Figs 5a–c) is not micron-sized pyrrhotite but rather greigite, which has no low-temperature magnetic transition (Dekkers *et al.* 2000).

The monitoring of LT-SIRM during warming shows sharp drops of magnetization for the three samples (Fig. 6). More specifically, the loss of remanence exceeds 90 percent from 5 to 30 K for samples 5S and 17S, which is less marked in sample 3S. This drastic loss has two explanations: (1) it can be due to the Neel transition of siderite

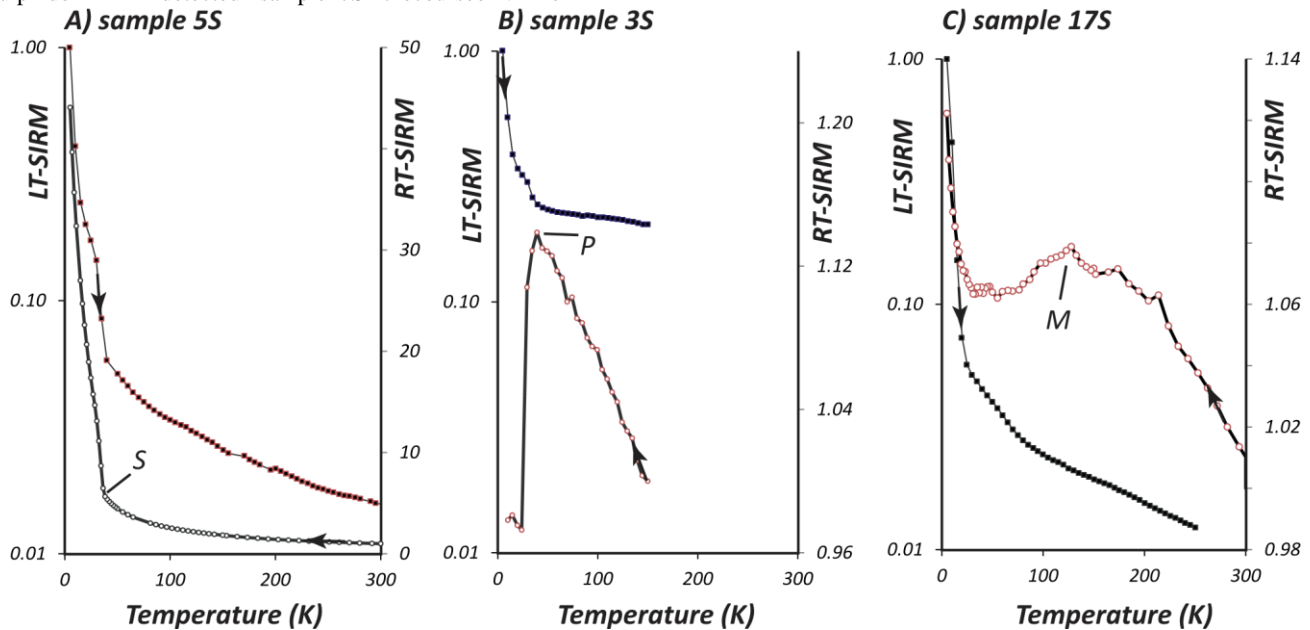


Figure 6. Low-temperature behaviour of saturated isothermal remanent magnetization (SIRM) acquired at room temperature (RT-SIRM, open symbols) and at low temperature (LT-SIRM, full symbols). (a) The sharp increase of RT-SIRM near ~ 40 K indicates the occurrence of siderite (S, Neel temperature of 39 K). This magnetic transition is also observed when warming the LT-SIRM. (b) The drop of RT-SIRM near ~ 35 K is the Besnus transition, indicating the occurrence of pyrrhotite (P). This transition is also observed when warming the LT-SIRM. (c) We identify a Verwey transition at 120 K which indicates the occurrence of stoichiometric magnetite (M). Note the increase of RT-SIRM near 35 K which is an indication of hyper-fine pyrrhotite and magnetite.

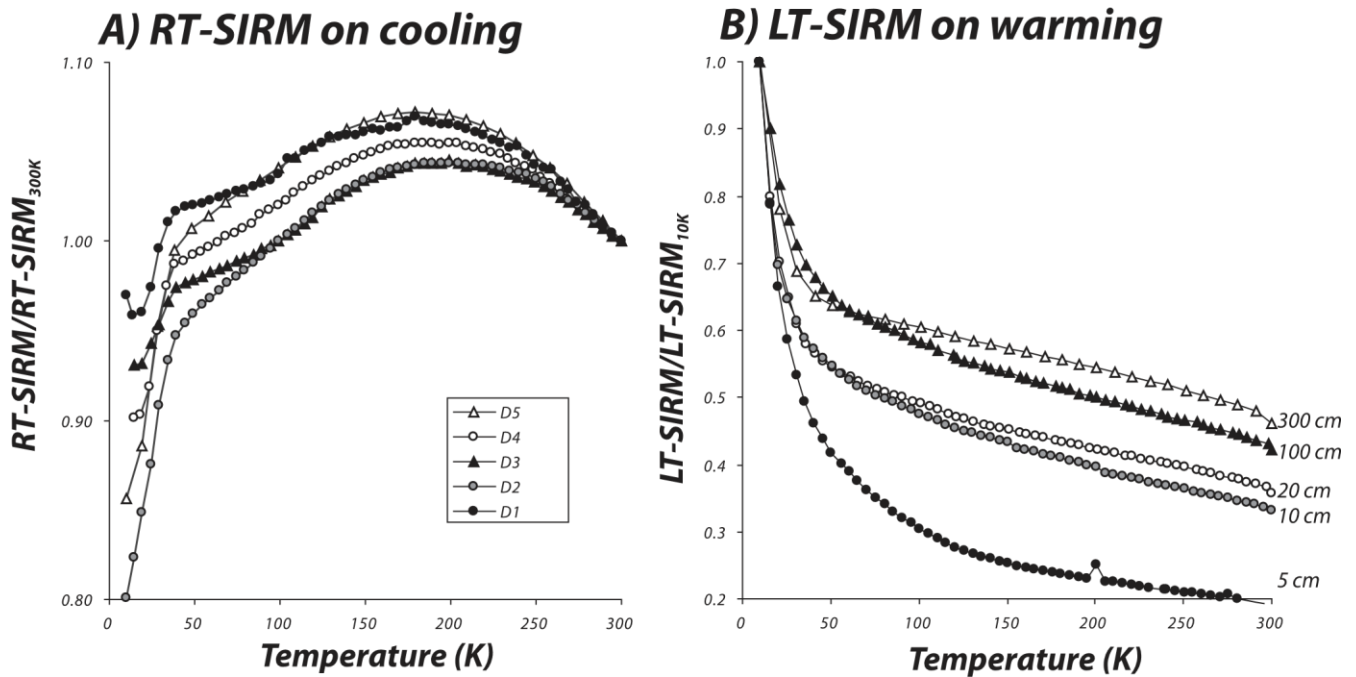


Figure 7. Low-temperature magnetic properties of argillaceous rocks along the three-profile next to a 1-m-thick dyke. (a) RT-SIRM. The drop of RT-SIRM near 35 K is the Besnus transition and points for the occurrence of $>1\mu\text{m}$ pyrrhotite. (b) LT-SIRM curves. The drop from 10 to 300K is varying at a function of distance of the dyke.

as for sample 5S, or (2) it can be attributed to the large occurrence of nano-sized fraction of magnetic minerals such as for sample 17S. These minerals acquire a remanence at very low temperature, and loose it when thermal energy is too high.

The low-temperature magnetic investigation of Cretaceous argillaceous rocks within the thermal aureole of a 1-m-thick dyke 9SD is pictured (Fig. 7). Sampling extends from 5 to 300 cm off the dyke. A Besnus transition was outlined and characterized by a drop of RT-SIRM at $\sim 35\text{K}$ and a bump at $\sim 200\text{K}$ for all samples whatever the distance to the dyke (Fig. 7a). Dekkers *et al.* (1989) suggested to study the reversibility of the RT-SIRM magnetic transition at 35K to gain information on the grain size. Cycling RT-SIRM by cooling and warming the sample collected at 5 cm from dyke was conducted, and a ratio $h/c = 0.6$ was obtained. This ratio suggests an average grain size of pyrrhotite of about $\sim 50\mu\text{m}$. The LT-SIRM demagnetization curves display a drop of remanence at a temperature below 40K (Fig. 7b). Remarkably, the magnitude of this drop is a function of the distance to the dyke; the drop is larger for the sample closer to the dyke, which suggests that the concentration of fine fraction of pyrrhotite is larger near the dyke.

5.2 Rock-Eval and reflectance

The TOC are lower than 2.9 percent, except for the Triassic sample 17S in which the content reaches 9.7 percent (Table 1). TOC are considered to be a bulk sedimentary parameter that represents the fraction of organic matter that survived degradation during both sedimentation and thermal diagenesis. It reflects the quantity of organic matter, keeping in mind that organically bound oxygen, hydrogen, sulphur and nitrogen also contribute to the sedimentary organic matter. Thus, 1 percent TOC usually corresponds to 1.25 percent of organic matter in thermally mature samples.

The HI is also generally low (often $<200\text{ mg HC/g TOC}$) in the studied samples, with a kerogen type usually based on marginally mature samples, indicating a predominance of Type III organic matter. However, samples such as 16Sb and 16Sd yield quite low HI-values (39 and 54 mg HC/g TOC, respectively) and can thus be classified into the Type IV organic matter, which represents highly oxidized organic matter, while Type III is derived from terrestrial higher plants.

The organic matter consists exclusively in higher plant debris of different origins (woody debris, spores and pollen grains) at different states of diagenetic and thermal alteration. The maceral analysis outlines that the organic matter mainly consists in small-sized ($<10\mu\text{m}$) particles having a rounded shape; some samples containing vitrinite particles with average sizes of about $50\mu\text{m}$. The rounded shape is a possible indication of inherited vitrinite particles.

An assessment of the level of maturity reached by the study samples is provided by T_{max} values determined by Rock-Eval pyrolysis and classical vitrinite reflectance measurements (Durand *et al.* 1986). Due to the very low quantity of hydrocarbons released during pyrolysis, the T_{max} values were determined only on half of the samples (Table 1). The values indicate that the sedimentary rocks reached different degrees of thermal evolution; most being located beyond the onset of the oil generation. The less mature samples are located less than 50km from the syenite intrusion (sites 2S and 11S, Table 1), where organic matter is still immature with respect to oil generation ($T_{\text{max}} < 420^\circ\text{C}$). The northern Triassic sites (16S and 17S) are only slightly mature, with T_{max} at about 435°C (Fig. 8). Samples from western part of the study area (sites 9S and 15S) are mature, with T_{max} values up to 468°C (Fig. 8, Table 1). Furthermore, some samples display a very high level of maturation and are overmature with respect to oil generation ($T_{\text{max}} > 465^\circ\text{C}$). It is clearly the case for the samples of site 8S, which were collected

near a basaltic sill. It is also probably the case for the samples of site 9SD where metric dyke delineated the outcrop.

The vitrinite reflectance data are scarce because the organic particles are usually too small to allow accurate measurements. Only six

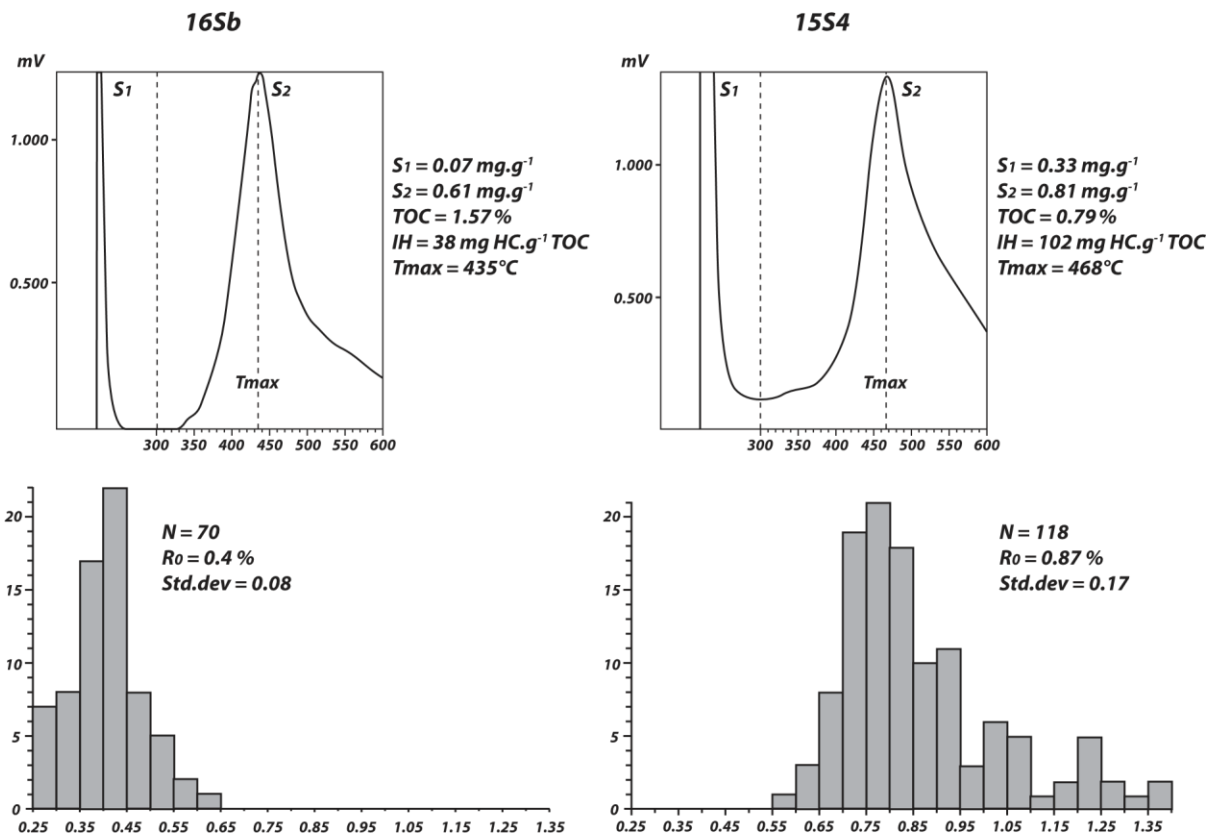


Figure 8. Two examples of early mature argillaceous rocks (Triassic argillaceous rocks 16S) and mature argillaceous rocks (Cretaceous argillaceous rocks 15S). Both T_{max} (upper curve) and the histogram of vitrinite reflectance are shown.

samples contained enough large vitrinite particles to allow statistical determination of their maturity degree with a good confidence (Table 1). The average R_0 is 0.53 ± 0.21 percent, with maximum and minimum values at 0.87 percent (site 15S) and 0.30 percent (site 9S), respectively. The R_0 measured at the sites 15S, 16S and 17S agrees well with the T_{max} data (Table 1, Fig. 8). However, an incoherence is underlined for sample 9S. The low reflectance ($R_0 = 0.30$ percent) measured at that site is in contradiction with the T_{max} value (468°C) indicating a mature degree.

5.3 XRD and K–Ar data

The XRD data of the $<2\mu\text{m}$ fractions document a combined content of illite and illite/smectite mixed layers (I-S) from 61 to 82 percent in the Cretaceous rocks, and from 7 to 51 percent in the Triassic rocks (Table 2). Triassic rocks are characterized by a significant occurrence of smectite and low illite and I-S contents. The content of kaolinite ranges from 3 to 10 percent in the Cretaceous rocks and from 12 to 16 percent in Triassic ones, whereas chlorite content ranges between 11 and 35 percent in all rocks. No clear trend was observed for the $<2\mu\text{m}$ mineralogical composition of the Cretaceous rocks, considering the different study sites. A systematic evolution is however observed at the local scale of the 9SD dyke (Table 2). Next to the dyke, the samples contain less illite (39 percent) and more I-S and kaolinite (26 and 12 percent, respectively). It results that the combined content illite + illite/smectite is significantly higher when the samples were taken away from the dyke. The I/I-S ratio, which outlines the relative amounts of well-crystallized illite relative to less crystallized I-S, is

relatively high (~ 10) in most of the samples next to the 9SD dyke and decreases when getting close to the intrusion. For the Cretaceous sites, all samples yield compositions ranging between the lowest values measured next to the dyke and the mean values away from it. However, most of the TGS samples yield low I/I-S ratios compare to those of the 9S site. Ratios lower than 2.5 were measured in the central part of the area (sites 10S and LG) whereas ratios higher than 2.5 (but lower than 10) were measured in the SE of the TGS (sites 1S, 2S and 4S). Samples containing only trace amounts or no I-S were not considered.

The ICI is quite similar for the entire set of samples with values ranging narrowly between 0.38 and 0.53 characterizing diagenetic to very-low grade metamorphism. No trend could be observed, meaning in turn that this information about the thermal gradient of the different sedimentary sequences is not unequivocal over the entire region.

The K–Ar data of the $<2\mu\text{m}$ fractions range from 58 ± 2 to 134 ± 4 Myr for the Cretaceous rocks and from 232 ± 8 to 266 ± 12

Myr for the Triassic rocks (Table 2). The illite of the Triassic rocks is obviously detrital, based on K–Ar values above stratigraphic age, making difficult the assessment that secondary authigenic illite formed during burial or volcanic intrusive or extrusive. As both sites were collected near the traps in HWH (Fig. 2), we are inclined to conclude that the thermal effect of the traps was not penetrative enough to reset the K–Ar system of these illite-rich size fractions. By contrast, two groups of K–Ar ages emerge in the Cretaceous rocks: those with an average value older than Aptian time (~110 Myr) for the sites 2S, 4S, 10S, LG and 14S, and those with K–Ar ages younger than 110 Myr for the sites 1S, 6S, 9SD and 15S. These sites

magmatic intrusions, although a burial effect cannot be excluded. At site 6S, for instance, the samples were collected a few metres from top of a large sill (thickness not known; Fig. 4b), which could explain the young ages induced by a thermal flux generated by the intrusive body. Site 1S is the closest site of the large Kap Simpson syenite intrusion (Fig. 2), and it is not excluded that resetting of the illite fractions relates to this 36-Myr-old event. At site 15S, no field indications of volcanic intrusions were recorded at distances lower than tens of metres from sampling places. The T_{\max} value (468 °C) is also consistent with the hypothesis of burial or thermal aureole of a cryptic intrusion.

Table 2. Mineral composition and K–Ar data of the <2µm size fractions. I-S, illite-smectite mixed-layers; Chl, chlorite; Kaol, kaolinite; acc., accessory minerals. 9SD has been sampled at variable distance from a 1-m-thick dyke. Distance is indicated in centimetres from dyke.

Site	s (amount ±5 per cent) at								K ₂ O (per cent)	⁴⁰ Ar (per cent)	⁴⁰ Ar* (10 ⁻⁶ cm ³ g ⁻¹)	⁴⁰ Ar/ ³⁶ Ar	⁴⁰ K/ ³⁶ Ar (10 ⁻³)	Age Myr (±2σ)
	Illite	I-S	I/I-S	I+I-S	Chl	Chl	Kaol	acc.						
1S	56	21	2.7	77	–	13	10	εqz	3.83	41.04	8.75	501	49.913	69.5 (1.9)
2S	47	14	3.4	61	–	32	7	εqz	3.87	31.86	16.35	434	18.125	126.5 (3.5)
4S	52	12	4.3	64	–	35		εqz, εfelds	4.10	58.97	15.82	720	61.014	115.8 (3.1)
LG	45	22	2.0	67	–	26	7	εqz, εfelds	4.05	48.11	16.64	569	36.911	123.3 (3.3)
6S	69			69	–	28	3	εqz, εfelds	4.51	41.09	11.13	502	46.306	74.9 (1.9)
9SD1–5	39	26	1.5	65	–	23	12	εqz, εfelds						
9SD2–20	67	7	9.6	74	–	26		εqz, εfelds	4.43	45.62	8.65	543	70.34	57.5 (1.5)
9SD3–100	67	6	11.2	73	–	27		εqz, εfelds	4.62	48.18	9.52	570	73.861	62.8 (1.5)
9SD4–10	58	7	8.3	65	–	35		εqz, εfelds						
9SD5–300	72	5	14.4	77	–	19	4	εqz, εfelds	4.35	52.43	9.97	621	78.739	69.7 (1.8)
10S	42	24	1.8	66	–	34		εqz	3.69	30.15	16.55	423	15.767	134.0 (3.8)
14S	73			73	–	24	3		6.32	82.07	26.69	1648	177.535	126.4 (2.4)
15S	48	34	1.4	82	–	18		εqz, εfelds	2.79	32.21	7.96	436	27.268	86.4 (2.8)
16S	33	18	1.8	51	–	33	16	εqz	2.85	37.27	22.84	471	12.144	232.8 (7.5)
17S	7			7	70	11	12		0.54	4.92	4.99	311	0.918	265.8 (12.2)

span Albian to Cenomanian time. Ages younger than 110 Myr imply alteration of the initial K-bearing clay-type minerals, in addition to authigenesis of new crystals most probably induced by the 55-Myr-old basaltic intrusion and/or the 36 Myr-old emplacement of the syenite plutons. On the other hand, K–Ar data older than Aptian time suggest a dominant detrital origin of illite that is likely in the <2µm fractions. The samples 9SD next to the metric dyke yield K–Ar ages (70–78 Myr, Table 2) that are younger than the depositional age and the ‘memory age’ of the detrital components. On the basis of previous studies on similar sediments cut by volcanic dykes (Clauer *et al.* 1995; Techer *et al.* 2001, 2006), it can be considered that the K–Ar value for the <2µm fraction closest to the dyke probably reflects the age of the intrusion event, at about 58 Myr. This age is in good agreement with the 55 Myr obtained by ⁴⁰Ar/³⁹Ar dating basaltic intrusions in TGS (Price *et al.* 1997). Based on this, it is possible that young illite K–Ar ages at the sites 1S, 6S and 15S are triggered by

6 DISCUSSION

The study indicates that the magnetic minerals of argillaceous rocks of eastern Greenland margin consist in an assemblage of iron oxides (magnetite) and iron sulphides (pyrrhotite and greigite). These minerals, magnetite and greigite, have also been described in the Cretaceous rocks from the western Greenland margin (Abdelmalak *et al.* 2012). In both margins, there is also evidence of nano-sized pyrrhotite. However, micron-sized pyrrhotite, that is carrying a remanence at room temperature, is only detected along the western margin.

The formation of micron-sized pyrrhotite in sediments is generally related to temperature elevation in anoxic conditions (Rochette 1987). In burial conditions, occurrence of pyrrhotite may be an indication of burial temperature >200 °C (Crouzet *et al.* 2001; Schill *et al.* 2002). In non-standard conditions of temperature elevation, like in the thermal aureole of a magmatic intrusion, several studies reported formation of pyrrhotite (Gillett

2003; Wehland *et al.* 2005; Ledevin *et al.* 2012). There is therefore a need to evaluate burial conditions of the eastern margin of Greenland to better understand the origin of pyrrhotite.

Fig. 9 shows the burial indicators. Apart sites 8S and 9SD, where Rock-Eval data suggest that organic matter is overmature ($T_{\max} > 500$ °C, Table 1), all burial indicators suggest that the organic matter is immature to mature (365 °C $< T_{\max} < 468$ °C, 0.3 percent $< R_0 < 0.9$ percent, $0.53 > ICI > 0.38$; Table 2). According to the experimental calibration curves of Sweeney & Burnham (1990), $R_0 < 0.9$ percent values indicate that the maximum temperature reached by the argillaceous rocks is < 150 °C, which is consistent with the maximum temperature obtained by Thomson *et al.* (1999) in Triassic and Jurassic rocks of the region. Additional evidence for low burial is provided by the detrital age of illite for Cretaceous rocks. Of eight localities studied, five localities have ages > 116 Myr (Table 2, Fig. 9).

The Triassic argillaceous rocks of the HWH peninsula provide good cases of immature organic matter ($R_0 < 0.4$ percent, $T_{\max} < 440$ °C, detrital age of illite > 233 Myr; Fig. 8). These argillaceous rocks are at the farthest distance from Kap Parry and Kap Simpson syenite intrusions (Fig. 8). At site 17S, the rock magnetic investigation showed the occurrence of magnetite and greigite. A similar magnetic assemblage has been reported by Abdelmalak *et al.* (2012) in Cretaceous rocks from the western margin. These authors also stated that this magnetic assemblage is consistent with immature to early mature organic matter. We are therefore inclined to consider that the Triassic argillaceous rocks from HWH were not impacted by the thermal aureole of the magmatic intrusion. By the way, it is noteworthy that the overlying kilometre thick traps have no apparent impact on either the magnetic assemblage or the maturity indicators.

South to HWH, when approaching the Kap Parry and Kap Simpson syenite, the organic matter of the Cretaceous rocks is immature to early mature, as indicated by vitrinite reflectance data ($R_0 < 0.9$ percent). However, the Rock-Eval data display a variability (Fig. 9) that is somehow larger than the range of the Rock-Eval data from Upper Triassic–Lower Jurassic Kap Stewart Formation of Jameson Land (440 °C $< T_{\max} < 446$ °C; Krabbe 1996). This variability suggests a possible impact of thermal aureoles, especially at the sites 8S and 9S (Fig. 9). However, the lowest values of T_{\max}

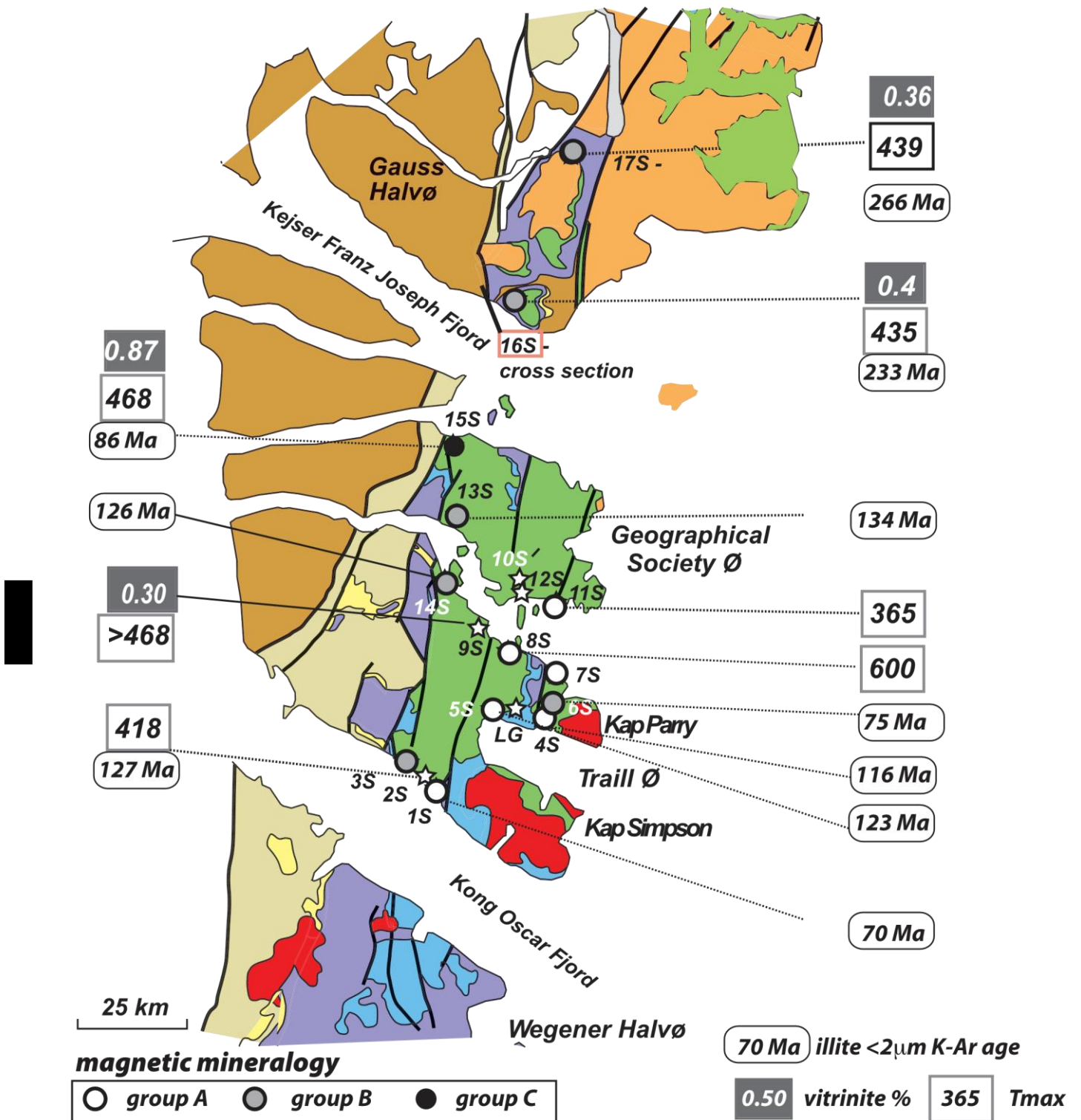


Figure 9. Map showing the maturity parameters (vitrinite R_0 , Rock-Eval T_{max}) obtained in this study. K–Ar of <2 mm illite is indicated. The magnetic mineralogy, based on the assemblage of pyrrhotite and magnetite is also shown.

(<420 °C) are located near the Kap-Simpson and Kap-Perry syenites. It is therefore, possible that the Rock-Eval data are equivocal and inconclusive. From data set generated here, neither vitrinite data, nor Rock-Eval data indicate relevant anomalies that map the thermal aureole of the syenite. Actually, the presence of

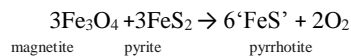
the thermal aureole is rather suggested by K–Ar data. Young illite ages <75 Ma are observed at the sites 1S and 6S, which are close to the intrusion of Kap Simpson and Kap Perry (Fig. 9), requiring concomitant formation of illite with the syenite intrusion.

Therefore, the pyrrhotite detected in the Cretaceous argillaceous rocks is possibly related to the thermal aureole of intrusion. At local scale, the 3-m profile in Cretaceous sediments near the 1-m-thick dyke (Fig. 7a) indicates the predominance of

micron-sized pyrrhotite, without evidence of magnetite. This magnetic assemblage is observed in argillaceous rocks for burial temperature exceeding 250 °C (Schill *et al.* 2002). Thus, it cannot be excluded that pyrrhotite is likely due to the magmatic intrusion.

For samples with a dominating pyrrhotite signal, demagnetization of NRM yields a diagnostic pattern (Fig. 5a). It is characterized by a plateau from room temperature to ~320 °C, followed by an abrupt decrease (Figs 5a and b). This feature is observed at the sites 1S, 4S, 5S, 7S, 8S and 11S (samples of the groups A, Fig. 9). These sites frame the Kap-Perry and Kap-Simpson syenitic intrusions within ~20km. Within the thermal aureole of 5-km-wide granitic intrusion, Gillett (2003) observed a similar behaviour during thermal demagnetization of the NRM from sediments, that he named 'square-shouldered'. Otofujii *et al.* (2003) observed also 'square-shouldered' NRM demagnetization patterns in limestones within the thermal aureole of a ~40km granitic intrusion (Kitakami, Japan).

The 'square-shouldered' pattern implies that the spectrum of unblocking temperature of pyrrhotite is restricted to values near the Curie temperature (~340 °C). In other words, this type of pattern suggests homogenous distribution of large pyrrhotite; provided that the largest unblocking temperatures are observed in the largest crystals. Gillett (2003) envisioned that pyrrhotite formed at the expense of magnetite and pyrite (FeS₂), at temperatures lower than 200 °C, according to the reaction:



Thermal demagnetization of NRM shows that the content of magnetite is limited in argillaceous rocks from group A. Moreover, the absence of Verwey transition for samples near the dyke 9SD indicates that magnetite is not detectable. Then, it can be assumed that pyrrhotite formed at the expense of magnetite. Gillett (2003) also argued that formation of pyrrhotite is not triggered by external intrusion fluids, but more locally by hydrous phases over millimetric distances. Formation of micron-sized pyrrhotite is then probably triggered by dehydration of clays (e.g. Vidal *et al.* 2009). Elevation of temperature is not accompanied by an elevation of pressure, and thus dehydration of clays can be more efficient.

7 CONCLUSION

The thermal aureole of magmatic intrusions in argillaceous rocks in the basin of the eastern Greenland volcanic margin was examined in detail. Maturity indicators reveal that the organic matter is immature to mature, without clear impact of the thermal aureole of the nearby magmatic intrusions:

- (i) The vitrinite reflectance is ranging from 0.3 to 0.9 percent.
- (ii) The Rock-Eval data provides T_{max} between 365 and 468 °C.
- (iii) The index of illite crystallinity is >0.38, without clear evidence of neofomed illite within the thermal aureole.
- (iv) A detrital K–Ar age of illite is observed in five out of eight studied sites.

However, local anomalies of Rock-Eval data or young illite K–Ar ages indicate possible imprints of a thermal aureole. This is especially well documented near a 1-m-thick dyke. With this level of maturity, the argillaceous rocks should have a magnetic assemblage

consisting essentially of stoichiometric magnetite. This magnetic assemblage is observed in Triassic argillaceous rocks from HWH, far from syenite intrusion. However, rock magnetic investigation shows the occurrence of micron-sized pyrrhotite in Cretaceous argillaceous rocks at a distance compatible with the thermal aureole of magmatic intrusions. Pyrrhotite is unambiguously detected due to the observation of the Besnus transition at ~35K. Thermal demagnetization of the NRM provides a diagnostic 'square-shouldered'

pattern, with a drastic drop of magnetization near the Curie temperature of pyrrhotite. This behaviour, already observed in other plutons aureoles, is indicative of a rather narrow distribution of micro-sized pyrrhotite, which develops at the expense of magnetite.

This study demonstrates that it is possible to detect the thermal aureole of unexposed magmatic intrusion by applying magnetic investigation. A promising application would be a precise delineation of the thermal aureole resulting from a magmatic intrusion.

ACKNOWLEDGEMENTS

The 2006 field trip was funded by GDR-Marge and IPEV (Program 290). Logistics was taken care of by F. Delbart. F. Pincsondu Seland E. Brossier skipped the 'Vagabond' and helped collecting samples. MPMS measurements were performed at the Institut Neel (France) and at the Institute of Rock Magnetism (IRM; Minneapolis, USA). CA benefited from an IRM grant. M. Mattei, an anonymous reviewer and E. Petrovski (associated editor) are thanked for their constructive reviews.

REFERENCES

- Abdelmalak, M.M., Aubourg, C., Geoffroy, L. & Lagoun-Defarge, F., 2012. A new oil-window indicator? The magnetic assemblage of argillaceous rocks from the Baffin Bay volcanic margin (Greenland), *AAPG Bull.*, **96**(2), 205–215.
- Aubourg, C. & Pozzi, J.P., 2010. Toward a new <250-C pyrrhotite-magnetite geothermometer for argillaceous rocks, *Earth planet. Sci. Lett.*
- Aubourg, C., Pozzi, J.-P. & Kars, M., 2012. *Burial, Argillaceous Rocks Remagnetization and Some Consequences for Magnetostratigraphy*, Geological Society, Special Publications, 371.
- Bishop, A.N. & Abbott, G.D., 1995. Vitrinite reflectance and molecular geochemistry of Jurassic sediments: the influence of heating by Tertiary dykes (northwest Scotland), *Organic Geochem.*, **22**(1), 165–177.
- Bonhomme, M.G., Thuizat, R., Pinault, Y., Clauer, N., Wendling, A. & Winkler, R., 1975. *Methodes de datation Potassium-Argon. Appareillage et technique*, Institut de Geologie Strasbourg.
- Bott, M.H.P., 1987. The continental margin of central east Greenland in relation to North Atlantic plate tectonic separation, *J. geol. Soc. Lond.*, **144**, 561–568.
- Brothers, L.A., Engel, M.H. & Elmore, R.D., 1996. The late diagenetic conversion of pyrite to magnetite by organically complexed ferric iron, *Chem. Geol.*, **130**, 1–14.
- Cairanne, G., Aubourg, C., Pozzi, J.-P., Moreau, M.G., Decamps, T. & Marolleau, G., 2004. Experimental chemical remanent magnetization in a

- natural claystone: a record of two magnetic polarities, *Geophys. J. Int.*, **159**, 907–916.
- Clauer, N., Rais, N., Schaltegger, U. & Pique, A., 1995. K-Ar systematics of clay-to-mica minerals in a multi-stage low-grade metamorphic evolution, *Chem. Geol.*, **124**, 305–316.
- Crouzet, C., Menard, G. & Rochette, P., 1999. High-precision three-dimensional paleothermometry derived from paleomagnetic data in an alpine metamorphic unit, *Geology*, **27**, 503–506.
- Crouzet, C., Rochette, P. & Menard, G., 2001. Experimental evaluation of thermal recording of polarity reversals during metasediments uplift, *J. geophys. Int.*, **145**, 771–785.
- Dam, G., Larsen, M. & Sonderholm, M., 1998. Sedimentary response to mantle plumes; implications from Paleocene onshore successions, *Geology*, **26**, 207–210.
- Dekkers, M.J., Mattei, J.-L., Fillion, G. & Rochette, P., 1989. Grain-size dependence of the magnetic behaviour of pyrrhotite during its low-temperature transition at 34K, *Geophys. Res. Lett.*, **16**(8), 855–858.
- Dekkers, M.J., Passier, H.F. & Schoonen, M.A.A., 2000. Magnetic properties of hydrothermally synthesized greigite (Fe₃S₄)-II high and low-temperature characteristics, *Geophys. J. Int.*, **141**, 809–819.
- Dunlop, D.J., 1995. Magnetism in rocks, *J. geophys. Res.*, **100**(B2), 2161–2174.
- Durand, B., Alpern, B., Pittion, J.L. & Pradier, B., 1986. Reflectance of vitrinite as a control of thermal history of sediments, in *Thermal Modelling in Sedimentary Basins*, pp. 441–474, ed. Burrus, J., Technip.
- Ellam, R.M., Upton, B.G.J. & Fitton, J.G., 1998. Petrogenesis of late stage magmatism at Hold with Hope, east Greenland, *Contrib. Miner. Petrol.*, **133**, 51–59.
- Espitalie, J., 1986. Use of T_{max} as a maturation index for different types of organic matter. Comparison with vitrinite reflectance, in *Thermal Modelling in Sedimentary Basins*, pp. 475–496, ed. Burrus, J., Technip.
- Espitalie, J., 1993. Rock Eval pyrolysis, in *Applied Petroleum Geochemistry*, pp. 237–261, ed. Bordenave, M.L., Technip.
- Frey, M., 1987. Very low-grade metamorphism of clastic sedimentary rocks, in *Low Temperature Metamorphism*, pp. 9–58, eds Frey, D. & Robinson, D., Blackie and Son, Ltd.
- Geoffroy, L., Aubourg, C., Callot, J.P. & Barrat, J.A., 2007. Mechanisms of crustal growth in large igneous provinces: the north Atlantic province as a case study, *Bull. geol. Soc. Am., Special Paper*, **430**, 747–774.
- Gernigon, L., Ringenbach, J.-C., Planke, S. & Le Gall, B., 2004. Deep structures and breakup along volcanic rifted margins: insights from integrated studies along the outer Vøring Basin (Norway), *Mar. Petrol. Geol.*, **21**, 363–372.
- Gillett, S.L., 2003. Paleomagnetism of the Notch Peak contact metamorphic aureole, revisited: pyrrhotite from magnetite+pyrite under submetamorphic conditions, *J. geophys. Res.*, **108**(B9), 2446.
- Hansen, K., Bergman, S.C. & Henk, B., 2001. The Jameson Land basin (east Greenland): a fission track study of the tectonic and thermal evolution in the Cenozoic North Atlantic spreading regime, *Tectonophysics*, **331**(3), 307–339.
- Hartz, E.H., Torsvik, T.H. & Andresen, A., 1997. Carboniferous age for the East Greenland “Devonian” basin: Paleomagnetic and isotopic constraints on age, stratigraphy and plate reconstructions, *Geology*, **26**(8), 675–678.
- Hong, C.-S., Huh, C.-A., Chen, K.-H., Lin, C.-H., Shea, K.-S. & Hsiung, K.-H., 2012. Pyrrhotite as a tracer for denudation of the Taiwan orogen, *Geochem. Geophys. Geosyst.*, **13**, Q08Z47, doi:10.1029/2012GC004195.
- Housen, B.A., Banerjee, S.K. & Moskowitz, B.M., 1996. Low-temperature magnetic properties of siderite and magnetite in marine sediments, *Geophys. Res. Lett.*, **23**(20), 2843–2846.
- Kars, M., Aubourg, C. & Pozzi, J.-P., 2011. Low temperature magnetic behaviour near 35 K in unmetamorphosed argillaceous rocks, *J. geophys. Int.*, **186**(3), 1029–1035.
- Kars, M., Aubourg, C., Pozzi, J.-P. & Janots, D., 2012. Continuous production of nanosized magnetite through low grade burial, *Geochem. Geophys. Geosyst.*, **13**, Q08Z48, doi:10.1029/2012GC004104.
- Katz, B., Elmore, R.D. & Engel, M.H., 1998. Authigenesis of magnetite in organic-rich sediment next to a dike: implications for thermoviscous and chemical remagnetizations, *Earth planet. Sci. Lett.*, **163**, 221–234.
- Krabbe, H., 1996. Biomarker distribution in the lacustrine shales of the Upper Triassic-Lower Jurassic Kap Stewart Formation, Jameson Land, Greenland, *Mar. Petrol. Geol.*, **13**(7), 741–754.
- Kubler, B., 1966. “La cristallinité de l’illite et les zones tout à fait supérieures du métamorphisme, Colloque sur les Etages Tectoniques,” La Baconniere, Neuchatel, pp. 105–122.
- Lanson, B., 1997. Decomposition of experimental X-ray diffraction pattern (profile fitting): a convenient way to study clay minerals, *Clays Clay Miner.*, **45**, 132–146.
- Lanson, B. & Besson, G., 1992. Characterization of the end of smectite-toillite transformation: decomposition of X-ray patterns, *Clays Clay Miner.*, **40**, 40–52.
- Ledevin, M., Arndt, N., Cooper, M.R., Earls, G., Lyle, P., Aubourg, C. & Lewin, E., 2012. Intrusion history of the Portrush Sill, County Antrim, Northern Ireland: evidence for rapid emplacement and high-temperature contact metamorphism, *Geol. Mag.*, **149**(1), 67–79.
- Lowrie, W., 1990. Identification of ferromagnetic minerals in rock by coercivity and unblocking temperature properties, *Geophys. Res. Lett.*, **17**(2), 159–162.
- Mathiesen, A., Bidstrup, T. & Christiansen, F.G., 2000. Denudation and uplift history of the Jameson Land basin, East Greenland—constrained from maturity and apatite fission track data, *Glob. Planet. Change*, **24**, 275–301.
- Moore, D.M. & Reynolds, R.C., 1997. *X-ray diffraction and Identification of Clay Minerals*, 2nd edn, Oxford, 378pp.
- Moreau, M.G., Ader, M. & Enkin, R.J., 2005. The magnetization of clay-rich rocks in sedimentary basins: low-temperature experimental formation of magnetic carriers in natural samples, *Earth planet. Sci. Lett.*, **230**, 193–210.
- Otofujii, Y., Takemoto, K., Haider Zaman, H., Nishimitsu, Y. & Wada, Y., 2003. Cenozoic remagnetization of the Paleozoic rocks in the Kitakami massif of northeast Japan, and its tectonic implications, *Earth planet. Sci. Lett.*, **210**, 203–217.
- Ozdemir, O., Dunlop, D.J. & Moskowitz, B., 2002. Change in remanence, coercivity, and domain state at low temperature in magnetite, *Earth planet. Sci. Lett.*, **194**, 343–358.
- Price, S.P., Brodie, J., Whitham, A.G. & Kent, R., 1997. Mid-Tertiary rifting and magmatism in the Traill Ø region, East Greenland, *J. geol. Soc. Lond.*, **154**, 419–434.
- Roberts, A.P., Chang, L., Rowan, C.J., Horng, C.-S. & Florindo, F., 2011. Magnetic properties of sedimentary greigite (Fe₃S₄): an update, *Rev. Geophys.*, **49**(1), RG1002, doi:10.1029/2010RG000336.
- Roberts, A.P., Chang, L., Heslop, D., Florindo, F. & Larrasoana, J.C., 2012. Searching for single domain magnetite in the “pseudo-single-domain” sedimentary haystack: implications of biogenic magnetite preservation for sediment magnetism and relative paleointensity determinations, *J. geophys. Res.*, **117**(B8), B08104, doi:10.1029/2012JB009412.
- Rochette, P., 1987. Metamorphic control of the magnetic mineralogy of black shales in the Swiss Alps: toward the use of “magnetic isogrades”, *Earth planet. Sci. Lett.*, **84**, 446–456.
- Rochette, P., Fillion, G., Mattei, J.-L. & Dekkers, M.J., 1990. Magnetic transition at 30–40 Kelvin in pyrrhotite: insight into a widespread occurrence of this mineral in rocks, *Earth planet. Sci. Lett.*, **98**, 319–328.

- Scheck-Wenderoth, M., Raum, T., Faleide, J.I., Mjelde, R. & Horsfield, B., 2007. The transition from the continent to the ocean: a deeper view on the Norwegian margin, *J. geol. Soc. Lond.*, **164**, 855–868.
- Schill, E., Appel, E. & Gautam, P., 2002. Towards pyrrhotite/magnetite geothermometry in low grade metamorphic carbonates of the Tethyan Himalayas (Shiar Khola, Central Nepal), *J. Asian Earth Sci.*, **20**, 195–201.
- Schindwein, V. & Jokat, W., 1999. Post-collisional extension of the east Greenland caledonides: a geophysical perspective, *Geophys. J. Int.*, **140**, 559–567.
- Scott, R.A., 2000. Mesozoic-Cenozoic evolution of east Greenland: implications of a reinterpreted continent–ocean boundary location, *Polarforschung*, **68**, 83–91.
- Stach, E., Mackowsky, M.T., Teichmüller, M., Taylor, G.H., Chandra, D. & Teichmüller, R.P., 1982. *Stach's Textbook of Coal Petrology*, Gebrüder Borntraeger, 535pp.
- Steiger, R.H. & Jäger, E., 1977. Subcommittee on geochronology: convention on the use of decay constants in geo- and cosmochronology, *Earth planet. Sci. Lett.*, **36**, 359–362.
- Stemmerik, L., Clausen, O.R., Korstgård, J., Larsen, M., Piasecki, S., Seidler, L., Surlyk, F. & Herkelsen, J., 1997. Petroleum geological investigations in East Greenland: project 'Resources of the sedimentary basins of North and East Greenland', *Geol. Greenland Surv. Bull.*, **176**, 29–38.
- Surlyk, F., Clemmensen, L.B. & Larsen, H.C., 1980. Post-Paleozoic evolution of the East Greenland continental margin, *Bull. Can. Petrol. Assoc. Mem.*, **7**, 611–645.
- Sweeney, J.J. & Burnham, A.K., 1990. Evaluation of a simple model of vitrinite reflectance based on chemical kinetics, *Am. Assoc. Petrol. Geol. Bull.*, **75**, 1279–1299.
- Techer, I., Lancelot, J., Clauer, N., Liotard, J.M. & Advocat, T., 2001. Alteration of a basaltic glass in an argillaceous medium: the Salagou dike of the Lodeve Permian Basin (France). Analogy with an underground nuclear waste repository, *Geochim. cosmochim. Acta*, **65**, 1071–1086.
- Techer, I., Rousset, D., Clauer, N., Lancelot, J. & Boisson, J.Y., 2006. Chemical and isotopic characterization of water-rock interactions in shales induced by the intrusion of a basaltic dike: a natural analogue for radioactive waste disposal, *Appl. Geochem.*, **21**, 203–222.
- Thomson, K., Green, P.F., Whitham, A.G., Price, S.P. & Underhill, J.R., 1999. New constraints on the thermal history of North-East Greenland from apatite fission-track analysis, *Bull. geol. Soc. Am.*, **111**(7), 1054–1068.
- Upton, B.G.J., Emeleus, C.H. & Hald, N., 1980. Tertiary volcanism in the northern E Greenland: Gauss Halvø and Hold with Hope, *J. geol. Soc. Lond.*, **137**, 491–508.
- Vidal, O., Dubacq, B. & Bousquet, R., 2009. Dehydration and stability of clays in the seismogenic zone, *Geophys. Res. Abstract*, **11**, EGU20093741.
- Weaver, R., Roberts, A.P. & Barker, A.J., 2002. A late diagenetic (synfolding) magnetization carried by pyrrhotite: implications for paleomagnetic studies from magnetic iron sulphide-bearing sediments, *Earth planet. Sci. Lett.*, **200**, 371–386.
- Wehland, F., Eibl, O., Kotthoff, S., Alt-Epping, U. & Appel, E., 2005. Pyrrhotite pTRM acquisition in metamorphic limestones in the light of microscopic observations, *Phys. Earth planet. Inter.*, **151**(1–2), 107–114.